JOURNAL OF THERMOPHYSICS AND HEAT TRANSFER
Vol. 9, No. 4, October–December 1995

Heat Transfer Measurement on a Waverider at Mach 10 Using Fluorescent Paint

T. Liu,* B. T. Campbell,* and J. P. Sullivan†
Purdue University, West Lafayette, Indiana 47906
and
J. Lafferty‡ and W. Yanta‡
U.S. Naval Surface Warfare Center, White Oak, Maryland 20910

The principles of the fluorescent paint technique for global surface temperature measurement are presented. This technique is used to measure the surface temperature and heat transfer on the windward side of a waverider model at Mach 10. The model used for calculation of heat transfer for hypersonic flow over an insulating layer is also discussed. Quantitative comparisons between heat transfer measured by the fluorescent paint and data obtained by thermocouples are made with good agreement. The heat transfer maps are able to clearly show not only transition from laminar to turbulent flow, but also movement of the transition line.

Nomenclature

c = specific heat at constant pressure
I = fluorescence intensity
k = thermal conductivity
L = insulating-layer thickness
p = pressure
q = heat flux
T = temperature
α = thermal diffusivity
θ = $T - T_{in}$
ρ = density

Subscripts
b = base
i = insulating layer
in = initial
r = reference
s = surface
w = wall
0 = total
∞ = freestream

Introduction

CONVENTIONAL techniques for surface heat transfer measurement, such as the thermocouple, thin-film gauge and slug calorimeter, have been widely used for many years in hypersonic wind-tunnel tests. However, since these sensors are distributed discretely on the test model surface, global surface heat transfer mapping cannot be easily obtained for the complicated three-dimensional flow over a hypersonic vehicle model. Therefore, novel methods for global surface temperature and heat transfer mapping become increasingly desirable in the fluid mechanics and heat transfer community. Some two-dimensional surface temperature mapping methods include IR imaging,[1] liquid crystal thermography,[2,3] and thermographic phosphors.[4,5] Recently, a surface temperature mapping technique using fluorescent coatings has been developed at Purdue University. The temperature-dependent fluorescent quantum efficiency of the rare-Earth chelate europium thenoyltrifluoroacetonate (EuTTA) has been exploited to visualize the surface temperature pattern produced by the leading-edge vortices of a delta wing, and to detect boundary-layer transition on a two-dimensional wing.[6] It was also used to make heat transfer measurement in shock/turbulent boundary-layer interactions.[7,8] This article presents the principles of the fluorescent paint technique and its application in surface heat transfer mapping for a waverider model at Mach 10.

Facility and Test Model

The experiment was conducted in the Naval Surface Warfare Center (NSWC) Hypervelocity Wind Tunnel no. 9. The tunnel is a blowdown facility that operates at Mach numbers of 8, 10, 14, and 16.5 with corresponding maximum Reynolds numbers per foot of approximately 50×10^6, 20×10^6, 3.8×10^6, and 3.2×10^6, respectively. The test cell diameter is 5 ft and the length is over 12 ft, which allows for testing of large model configurations.

Tunnel 9 uses nitrogen as the working fluid. During a typical run, the vertical heater vessel is used to pressurize and heat a volume of nitrogen to a predetermined pressure and temperature. The test section and vacuum sphere are evacuated to a low pressure and are separated from the heater by a pair of metal diaphragms. When the nitrogen in the heater reaches the proper temperature and pressure, the diaphragms are ruptured and the gas flows from the top of the heater and expands through the nozzle. As the hot gas exits the heater, cold gas from three pressurized driver vessels enters the heater base. The cold gas drives the hot gas in a piston-like fashion, thereby maintaining near-steady conditions in the test cell during the run. More detailed information concerning the facility can be found in Ref. 9. Nominal tunnel conditions for this test program are listed in Table 1.

The process used to generate the waverider shape is described in detail in Ref. 10. A modified version of the University of Maryland Axisymmetric Waverider Program (MAXWARP) code was used to generate a sharp-edged waverider optimized on a figure of merit that encompassed viscous lift-to-drag ratio, volume, and wetted area. The design conditions of Mach 14 and $Re_1 = 6.5 \times 10^6$ were chosen based upon

Presented as Paper 94-2484 at the AIAA 18th Aerospace Ground Testing Conference, Colorado Springs, CO, June 20–23, 1994; received Sept. 9, 1994; revision received March 22, 1995; accepted for publication March 24, 1995.

*Graduate Research Assistant, School of Aeronautics and Astronautics. Student Member AIAA.
†Professor of Aerodynamics, School of Aeronautics and Astronautics. Member AIAA.
‡Aerospace Engineer, Strategic and Space Systems Department. Member AIAA.

Table 1 Nominal test conditions

Mach no.	p_0, psia	T_0, °R	Re_∞, 1/ft	U_∞, ft/s	T_∞, °R	p_∞, psia	Dynamic pressure, psia	Angle of attack		Run time, s
9.7	1300	1840	2.0×10^6	4650	96	0.039	2.5	10 deg (t = 0–1.6 s)	10 to −25 deg (t = 1.6–2.3 s)	2.3

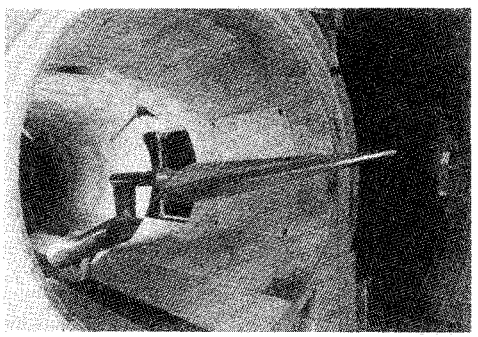

Fig. 1 Model mounted in tunnel 9.

the facility capabilities. The final design had an overall length of 39 in., a span of 16.161 in., and a base height of 6.839 in. The planform and base areas were 375.3 and 64.6 in.^{2}, respectively. The model had a leading-edge radius of 0.25 in.

The model was fabricated in eight parts. The body consisted of four sections manufactured from 6061-T6 aluminum. The nose, both leading edges, and the main cavity cover plate were manufactured from 17-4 PH stainless steel. A photograph of the model mounted in the tunnel is shown in Fig. 1. Additional information regarding the model design can be found in Ref. 11.

Surface static pressures were measured at 32 locations on the model with Kulite model XCW-062-5A transducers. Measurements of surface temperature rise were made using Medtherm model TCS-E-10370 coaxial thermocouples. The thermocouple materials were chromel and constantan. The gauges were cemented into the model using Loctite no. 271 adhesive and sanded to conform to the external contours; the sanding formed the thermal junction.

In addition to the analog filters used on all channels, the data were filtered during data reduction using a low-pass sixth-order Butterworth digital filter. A cutoff frequency of 10 Hz was used for filtering the tunnel supply temperature and pressure data, the test cell pitot data, and all of the model temperature and pressure gauge data. The data were filtered both forward and backward to prevent the introduction of time lag.

The millivolt output of each coaxial thermocouple was converted to surface temperature rise using the conversion factor for chromel-constantan thermocouples. A heating rate was computed from each temperature rise using a finite difference solution of the unsteady, one-dimensional, heat-conduction equation for a homogeneous planar slab of finite thickness, as discussed in Refs. 12 and 13. For locations on the model where the base metal was aluminum, the thermocouples were mounted in 17-4 PH stainless steel plugs. The lumped thermal properties of 17-4 steel, chromel, and constantan are essentially equivalent, justifying the assumption of material homogeneity. A uniform initial temperature was assumed, and the inside surface of the model was assumed to experience zero heat transfer. The measured temperature rise at the heated surface provided the remaining boundary condition needed to compute the temperature distribution within the slab. Temperatures were calculated at 50 node points in the slab, and the heating rate was computed from the temperature gradient at the surface and the thermal conductivity of the gauge material. Calculations were also performed with 20 and 100 nodes; these calculations showed that the solutions were converged with 50 nodes. It should be noted that the assumption of one-dimensional planar heat conduction was not valid for the gauges on the leading edge. For these gauges, a cylindrical implementation of the one-dimensional heat conduction equation was used.

Experimental Techniques

Temperature-Sensitive Fluorescent Paint

A schematic of the test configuration is shown in Fig. 2. The lower half of the waverider model's windward surface was covered with a white Mylar® film on which the fluorescent paint was applied. The model was mounted in tunnel no. 9 and illuminated with uv light to cause the paint to fluoresce. A charged coupled device (CCD) array camera is used to obtain intensity measurements over the surface. The signal from the camera is recorded with a VCR for later digitization. Detailed descriptions of the processes used during and after this experiment will be given below.

Fluorescence is one of the photoluminescence processes whereby the molecules of a substance absorb light of a particular wavelength and re-emit radiation of a longer wavelength by losing their excitation energy. The fluorescence process can be deactivated by so-called thermal quenching. Hence, the fluorescence quantum efficiency depends on temperature. A detailed discussion on photochemical processes of photoluminescence can be found in Ref. 14. The temperature dependence of the fluorescent intensity of many chemical compounds in different binders has been determined experimentally.[15] For the EuTTA in model airplane dope used in this study, Fig. 3 shows the relation between temperature T (°C) and intensity (8-bit counts) for the digitized fluorescent intensity images taken by the CCD camera used in the experiment. A fourth-order polynomial fit with a correlation coefficient of 0.999 is also plotted with the experimental data over a temperature range from 5 to 90°C. The polynomial is given by

$$I(T) = \sum_{n=0}^{4} a_n T^n = F(T) \tag{1}$$

where $a_0 = 164.1315$, $a_1 = -3.09987$, $a_2 = -1.44092 \times 10^{-3}$, $a_3 = 3.00562 \times 10^{-4}$, $a_4 = -1.39271 \times 10^{-6}$. The units of T in Eq. (1) are degrees Celcius. In order to eliminate the effects of uneven lighting, fluorophore concentration and paint-layer thickness, the relative intensity $I(T)/I(T_r)$ must be considered, where T_r is some reference temperature. Thus, a normalized form of the calibration relation is written

$$I(T)/I(T_r) = F(T)/F(T_r) \tag{2}$$

The calibration relation (2) can be used to obtain the temperature distribution on a surface, provided a reference image is taken at a known temperature. The reference image is usually obtained before the test begins and the reference temperature is taken to be the test section static temperature at this time. The procedure is to divide the image with an unknown temperature distribution by the reference image pixel-by-pixel. This yields the ratio $I(T)/I(T_r)$ for each pixel in the image. Since the reference temperature T_r is known, the temperature at each pixel location on the surface can be determined using the calibration relation (2). This procedure can

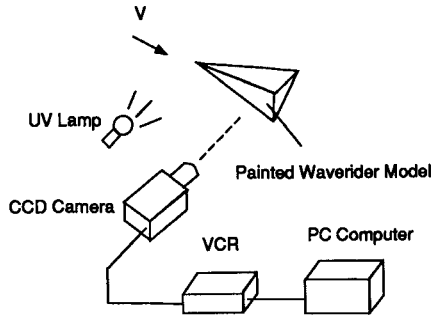

Fig. 2 Schematic of measuring system for fluorescent paint technique.

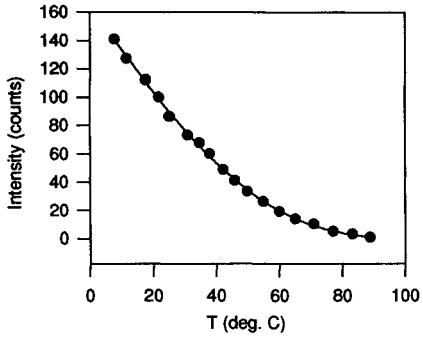

Fig. 3 Calibration curve for EuTTA-dope paint.

be carried out using a fairly simple computer program. Moreover, it should be mentioned that the EuTTA-dope paint does not exhibit any pressure sensitivity.

Heat Transfer Model

Figure 4 depicts a thin insulating layer on a thick metal base. Given a surface temperature distribution on the insulating layer, a data reduction model is needed to obtain heat transfer. If the insulating layer is thin enough and the temperature of the base does not change much during the short run, the heat flux q_s can be calculated using the discrete Fourier law:

$$q_s(t) = \frac{k_i[T_s(t) - T_b]}{L} \tag{3}$$

where T_s is the surface temperature on the insulating layer, T_b is the temperature at the interface between the insulating layer and the base material, and k_i and L are the thermal conductivity and thickness of the insulating layer, respectively. In general, T_b is an unknown time- and position-dependent function. In a short-duration test, however, T_b may be approximated by the initial temperature T_{in} if the base is made of a good thermal conductor. In the following paragraphs, we will examine the feasibility of using the difference expression (3) for heat transfer calculations in transient tests and estimate errors caused by the approximation $T_b \approx T_{in}$.

The differential form of the Fourier law is instantaneously valid. However, its discrete version (3) introduces a small time scale τ that is needed for creating a linear temperature profile across the thin insulating layer. The time scale τ is on the order of the heat penetration time ($\propto L^2/\alpha_i$), which is about 0.01 s for the 0.1-mm Mylar layer used in our experiments, where α_i is the thermal diffusivity of the insulating layer. When $t < \tau$, (3) tends to underestimate the heat transfer. In order to quantitatively validate the model (3), a comparison with a more accurate numerical calculation will be made for an idealized transient test case. Consider a 0.1-mm-thick Mylar film on a semi-infinite aluminum base. The surface temperature evolution is assumed to be a "2/3" power-law: $T_s - T_{in} = 40t^{2/3}$, where $T_{in} = 25$°C, because it has a weaker singularity in the rate of surface temperature change at $t = 0$ compared with the "1/2" power-law for a semi-infinite slab undergoing step heating. This presumed surface temperature development is used to simulate an actual variation in our experiments. Then, for comparison, the corresponding surface heat transfer is calculated by both a numerical method and the simple model (3) with the approximation $T_b \approx T_{in}$.

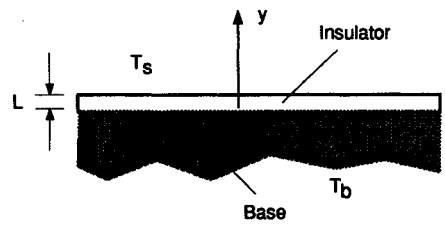

Fig. 4 Insulating layer on a semi-infinite base.

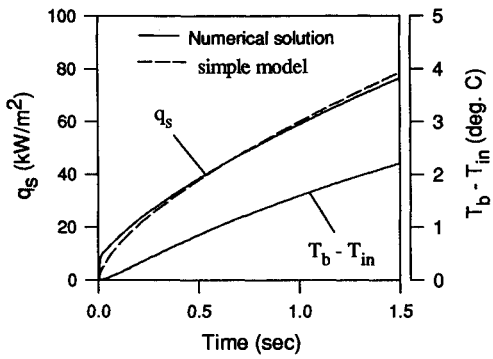

Fig. 5 Verification of the simple heat transfer model.

Since the insulating layer is usually thin, the one-dimensional time-dependent heat conduction equation, $(\partial/\partial t - \alpha\partial^2/\partial y^2)\theta(t, y) = 0$, is used, where $\theta(t, y) = T - T_{in}$, and $\alpha(k/c\rho)$ is the thermal diffusivity which is α_i for the insulating layer when $y > 0$ and is α_b for the base when $y < 0$. The subscripts i and b denote the insulating layer and base, respectively. Both the insulating layer and base material are assumed to have a constant temperature T_{in} at $t = 0$. The boundary conditions are that $\theta(t, L) = 40t^{2/3}$ and $\theta(t, -\infty) = 0$, where L is the thickness of the insulating layer. On the interface between the insulating layer and the base, the temperature is continuous. The heat flux continuity condition across the interface is that $k_i\partial\theta/\partial y = k_b\partial\theta/\partial y$ at $y = 0$. A standard fully implicit finite difference scheme is used to solve the above problem.[16] The Mylar insulating layer has $k_i = 0.15$ W/m-°C, $c_i = 1090$ J/kg-°C, and $\rho_i = 1420$ kg/m^3. The base material is aluminum with $k_b = 204$ W/m-°C, $c_b = 904$ J/kg-°C, and $\rho_b = 2700$ kg/m^3. Figure 5 shows the surface heat flux q_s (kW/m^2) computed by the numerical and simple methods. The temperature difference $T_b - T_{in}$ as a function of time computed by the numerical method is also plotted. It is found that the simple discrete Fourier law is able to produce heat transfer values that are in good agreement with those obtained with the more accurate numerical method, except at the very beginning ($t < 0.02$ s). At $t = 1.5$ s, the base temperature has changed about 2°C. Since the temperature difference across the insulating layer is on the order of 50°C, neglecting the variation in T_b leads to an error of approximately 4% in heat transfer calculations for an aluminum base. A larger error will occur at the stainless steel leading edge that has much smaller thermal conductivity. In this region, $T_b - T_{in}$ is about 7°C at $t = 1.5$ s. Accordingly, the simple heat transfer model has about 14% error near the leading edge. In this article, the simple model (3) is used for heat transfer data reduction due to its simplicity and reasonably good accuracy.

The effect of heat transfer from the back-surface of the waverider model must also be analyzed. It is possible that the heat transfer on the leeward side of the model could affect the surface temperature distribution on the windward side, thus corrupting our heat transfer calculation. In order to test this effect using a simple model, we will examine a slab of a finite thickness, which is suddenly heated by imposing heat fluxes on both sides (step functions). An analytical expression for the wall temperature T_w at the front-surface is given by (see Appendix)

$$T_w - T_{in} = \frac{2q_{s1}}{\sqrt{\pi\rho_b c_b k}}\sqrt{t} + \frac{q_{s1}}{\rho_b c_b H}F(t, \beta_1) + \frac{1.2q_{s2}}{\rho_b c_b H}F(t, \beta_2) \tag{4}$$

where T_{in} is the initial temperature, q_{s1} is the heat flux through the front-surface, q_{s2} is the heat flux through the back-surface, H is the thickness of the slab, $\beta_1 = 1.3225H^2/\alpha_b$ and $\beta_2 = 0.16H^2/\alpha_b$, the subscript b denotes the base (slab) material, and other notations have the conventional meanings. The function $F(t, \beta)$ is defined as

$$F(t, \beta) = [t + (\beta/2)]\text{erfc}(\sqrt{\beta}/2\sqrt{t}) - (\sqrt{\beta t}/\sqrt{\pi})\exp[-(\beta/4t)]$$

The physical meaning of each term in (4) is clear. The first term is the solution for a semi-infinite slab. The second term represents the effect of finite thickness, and the third term is the contribution from heat transfer on the back-surface. In our experiments, q_{s1} is typically 60 kW/m^2, and q_{s2} is 1 kW/m^2. For a 15-mm-thick aluminum slab, the combined effects of the finite thickness and back-surface heat transfer produce about 0.4°C deviation from the solution for a semi-infinite slab and leads to less than 1% error in the heat transfer calculation at $t = 1.5$ s. Hence, these effects are weak and will be neglected in a short-duration wind-tunnel test.

Uncertainty in heat transfer calculation is composed of errors in the measurement of the quantities in (3). With a large number of repeated calibration tests for the EuTTA-dope paint, we estimate an error of 0.7°C on surface temperature T_s. During the wind-tunnel test, deviation of T_b from T_{in} is about 2°C for the aluminum base. Thus, for a typical temperature difference of 50°C, the uncertainty in $T_s - T_b$ is about ±5%. The previously published values of k_i for Mylar from various sources show ±20% variation.[17] Therefore, applying the rss method to (3), we know that the combined uncertainty in heat transfer measurement is about ±21% on the aluminum base and ±25% on the stainless steel base. Note that a large portion of the error results from the uncertainty in evaluating k_i.

Description of the Experiment

A bottom view of the waverider model and coordinate locations of the thermocouples are shown in Fig. 6. Thermocouples for making heat transfer measurements are distributed on the surface of the upper half of the model. A 0.1-mm-thick white Mylar insulating layer covered the lower half of the windward side of the model, from the centerline to the outboard edge. The EuTTA-dope paint (about 10 μm thick) is brushed on the insulating layer for temperature mapping. A schematic representation of the fluorescent paint system is shown in Fig. 2. Ultraviolet illumination to excite the paint into emission was provided by four 40-W fluorescent black lights. Two CCD cameras, one viewing the front and one the back of the model, were used to image the luminescent surface. The images of the fluorescent paint were recorded with a VCR and then later digitized with a frame-grabber board with 256 gray level resolution (8 bits) and 512 × 512 pixel spatial resolution. The spatial resolution is about 1 mm. In order to obtain surface temperature maps, each image must be divided (normalized) by a reference image taken at a known ambient temperature prior to starting the tunnel, because the calibration relations correlate relative intensity with temperature. Conversion of fluorescent intensity into temperature is made using the calibration relation (2). Heat flux is then calculated using the simple model (3).

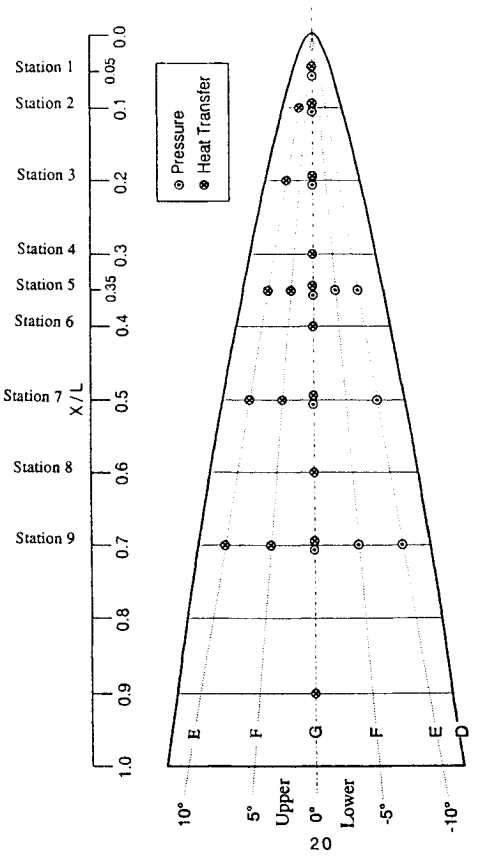

Fig. 6 Instrumentation locations on bottom of waverider model.

Results

The experiment was run at a freestream Mach number of 10 (9.7 ± 0.12 more precisely), average total pressure p_0 of 1300 psia (1250–1350 psia), and average total temperature T_0 of 1840°R (1700–1900°R). During the first 1.6 s of the test, the angle of attack was fixed at 10 deg. Then, the angle of attack swept from 10 to −25 deg. Nominal test conditions are listed in Table 1. Figure 7 shows windward-side heat transfer maps of the lower half of the waverider (58% of the total length is shown in the images) at $t = 0.27$, 0.37, 0.57, 0.77, 1.04, and 1.24 s after the wind tunnel starts to run. The gray intensity bar in Fig. 7 denotes heat flux in kW/m^2. The bright regions represent high heat transfer and dark regions represent low heat transfer. In these maps, the low heat transfer region (dark region) downstream of the leading edge corresponds to laminar flow. Transition from laminar to turbulent flow can be easily identified by the abrupt change from low to high heat transfer. A salient feature indicated in these maps is that the transition line moves toward the leading edge after $t = 0.77$ s, such that the dark laminar region diminishes as time elapses. Note that at the leading edge where three-dimensional conduction in the base may prevail, the heat transfer data are not accurate since the aforementioned data reduction procedure is no longer valid.

For the application of the fluorescent paint technique in hypersonic flow tests, the effect of the thickness of the insulating layer on measurement accuracy needs to be understood. For this purpose, patches composed of single (0.05 mm), double (0.1 mm), and triple (0.15 mm) Mylar film layers were placed on the back of the model near location T9E.

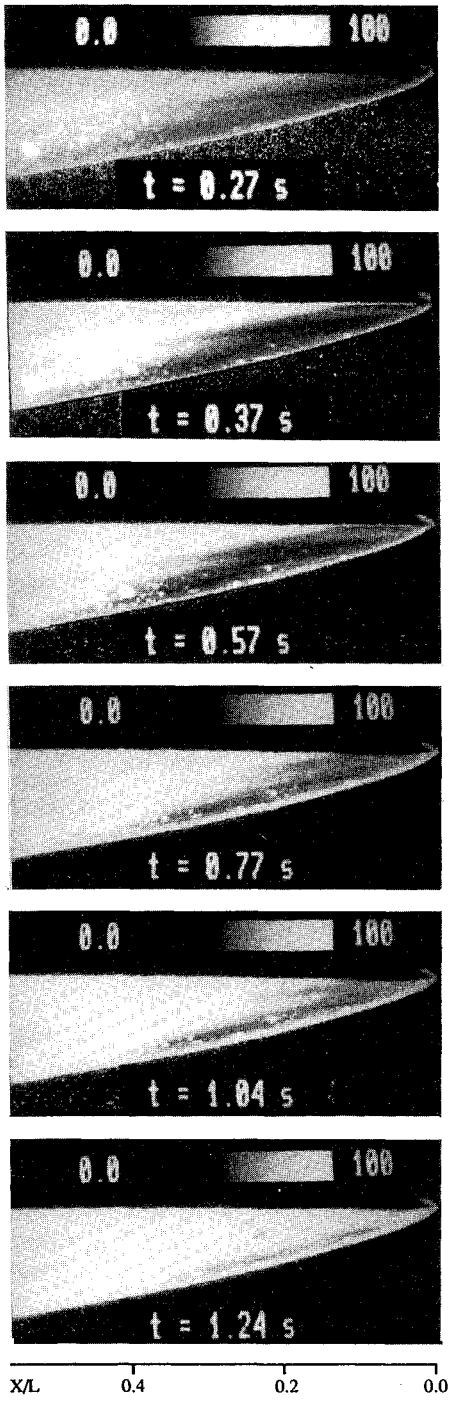

Fig. 7 Windward side heat transfer maps of waverider. The gray intensity bar units are kW/m².

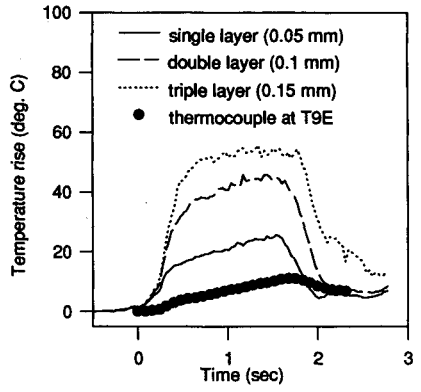

Fig. 8 Effect of insulating layer thickness on measurement of surface temperature.

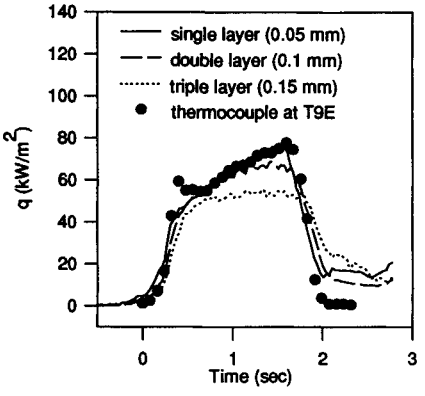

Fig. 9 Effect of insulating layer thickness on measurement of surface heat transfer.

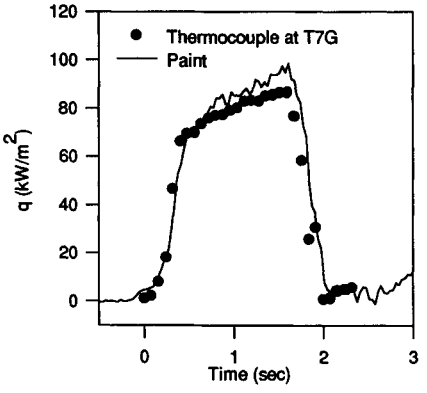

Fig. 10 History of surface heat transfer at T7G.

Here, T9E denotes the thermocouple at station 9 along ray E (see Fig. 6). The time evolution of the surface temperature rise and heat transfer measured on these layers are plotted in Figs. 8 and 9, respectively. The temperature rise and heat transfer measured by the thermocouple at T9E are also plotted for comparison. The surface temperatures on the insulating layers are much higher than those measured by the thermocouple mounted in a stainless steel plug, because the thermal conductivity of the insulating layers is much lower than that of stainless steel. The heat transfer on the single and double layers measured by the fluorescent paint is in agreement with the data obtained by the thermocouple at T9E. However, the data for the triple layer is not very good. Since the triple layer is so thick and the surface temperature is so high there, the temperature sensitivity of the paint is worsened, the signal-to-noise ratio (SNR) is reduced, and the temperature measurement is degraded. Furthermore, the simple model (3) may not be accurate for the thick layer.

Figure 10 shows a typical heat transfer evolution computed by the simple model (3), where k_i/L is 1.5×10^3 W/m²-°C. The heat transfer history obtained by the fluorescent paint is in agreement with that given by the thermocouple at T7G. The paint measurements were taken from a location of mirror symmetry to the thermocouple at T7G. The error in the location of the paint measurement point relative to the thermocouple is less than 1%. At locations T5G through T7G and T7F where the flow is turbulent, the general trend of heat transfer evolution is similar and quantitative comparison with data obtained by the thermocouples is good. At these locations, heat transfer increases rapidly immediately after the wind tunnel starts and then levels off after steady flow conditions are reached. At a time of about 1.6 s, the heat

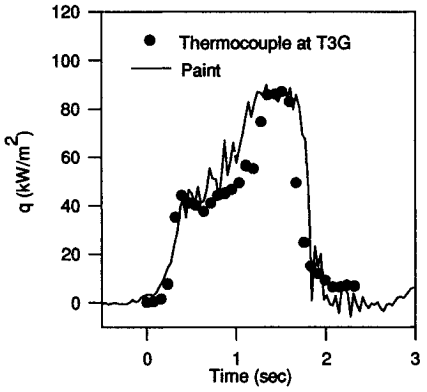

Fig. 11 History of surface heat transfer at T3G.

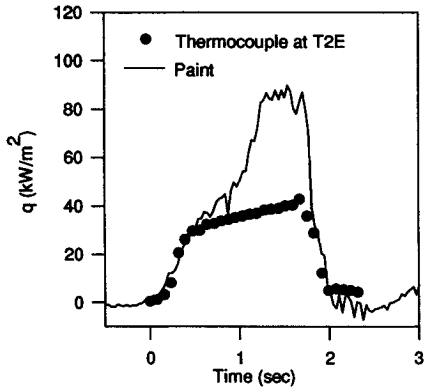

Fig. 12 History of surface heat transfer at T2E.

transfer decreases rapidly due to the sudden pitching of the model (the angle of attack swept from 10 to −25 deg). However, a different behavior in the heat transfer history can be seen in the data from location T3G near the tip of the model, as shown in Fig. 11. Heat transfer rapidly increases to about 40 kW/m^2 and levels off until $t = 1$ s, when it increases again to 90 kW/m^2. The second rise in heat transfer may be attributed to movement of the transition line towards the leading edge. The flow at location T3G is initially laminar and becomes turbulent later due to the movement of the transition line at $t = 1$ s. This appears in the data as a large increase in heat transfer at $t = 1$ s.

At locations T2E in the lower half, the heat transfer measured by the paint, when $t > 0.7$ s, becomes increasingly larger than that obtained by the thermocouple at the symmetrical location in the upper aluminum half (see Fig. 12). This difference or asymmetry is attributed to the movement of the transition line towards the leading edge. The heat transfer visualization in Fig. 7 indicates that the transition line starts to move roughly at $t = 0.7$ s. This time corresponds to the instant at which the heat transfer in the lower half deviates from the thermocouple data at T2E in the upper half. The heat transfer evolution observed at T3E and T5E also shows similar behavior. Although the reasons for the difference in transition location between the upper and lower half parts of the model remain unknown, it is possibly due to the destabilizing effect of increasing surface temperature on the lower half, small yaw angle, surface roughness, and freestream condition variation, etc.

Conclusions

The fluorescent paint technique for remote global temperature and heat transfer mapping has been developed and used to visualize and measure surface heat transfer on a waverider model at Mach 10. From the successive fluorescence intensity images, the surface heat transfer history is calculated based on a simple data reduction model. The heat transfer values measured by the fluorescent paint are in good agreement in many cases with the thermocouple data. The heat transfer maps of the windward side of the waverider model clearly indicate flow transition near the leading edge and movement of the transition line.

Appendix: Heat Transfer Analysis of a Slab with Finite Thickness

Consider a slab with a finite thickness H. The slab undergoes a heating process in which heat fluxes q_{s1} and q_{s2} are suddenly imposed on surfaces 1 and 2, respectively. The problem of interest is to obtain an expression for the wall temperature T_w on surface 1. The governing equation is $(\partial/\partial t - \alpha\partial^2/\partial x^2)\theta(t, x) = 0$, where $\theta(t, x) = T(t, x) - T_{in}$, T_{in} is the initial temperature and $\alpha(k/c\rho)$ is the thermal diffusivity of the slab material. The x coordinate originates from surface 1 and points towards surface 2. The initial condition is that $\theta(0, x) = 0$. The boundary conditions are that $q_{s1}H(t) + k\partial\theta/\partial x = 0$ at $x = 0$ and $q_{s2}H(t) - k\partial\theta/\partial x = 0$ at $x = H$, where $H(t)$ is the Heaviside function. In order to solve this problem, the Laplace transform, $\Theta(s, x) = La(\theta)$, is used, where La denotes the Laplace transform operator and s is the complex variable in La. Applying the Laplace transform to the equation and the boundary conditions, we obtain the transformed wall temperature at surface 1 ($x = 0$)

$$\Theta_w = \Theta(s, 0) = (q_{s1}\sqrt{\alpha}/ks^{3/2})\coth(\sqrt{s/\alpha}H) + (q_{s2}\sqrt{\alpha}/ks^{3/2})\operatorname{csch}(\sqrt{s/\alpha}H)$$

In order to take the analytical inverse of the Laplace transform, we use the following approximations: $\coth(x) \approx 1 + \exp(-1.15x)/x$ and $\operatorname{csch}(x) \approx 1.2\exp(-0.4x)/x$. These approximations have less than 1% errors. Finally, the inverse transform yields expression (4) for the wall temperature $\theta_w(t) = T(t, 0) - T_{in}$.

References

[1]Gartenburg, E., and Robert, A. S., "Twenty-Five Years of Aerodynamics Research with Infrared Imaging, a Survey," Thermosense XIII, An International Conference on Thermal Applications and Image Diagnostic, Orlando, FL, 1991.

[2]Jones, T. V., and Hippensteele, S. A., "High Resolution Heat Transfer Coefficient Maps Applicable to Compound-Curve Surface Using Liquid Crystals in a Transient Wind Tunnel," NASA TM 89855, 1988.

[3]Hippensteele, S. A., Russel, L. M., and Stepka, F. S., "Evaluation of a Method for Heat Transfer Measurements and Thermal Visualization Using a Composite of a Heater Element and Liquid Crystals," *Journal of Heat Transfer*, Vol. 105, Feb. 1983, pp. 184–189.

[4]Buck, G. M., "Automated Thermal Mapping Technique Using Chromatic Image Analysis," NASA TM 101554, 1989.

[5]Buck, G. M., "An Imaging System for Quantitative Surface Temperature Mapping Using Two-Color Thermographic Phosphors," 34th International Instrumentation Symposium, Albuquerque, NM, 1988.

[6]Campbell, B. T., Liu, T., and Sullivan, J. P., "Temperature Measurement Using Fluorescent Molecules," Sixth International Symposium on Applications of Laser Techniques to Fluid Mechanics, Lisbon, Portugal, 1992.

[7]Liu, T., Campbell, B. T., and Sullivan, J. P., "Thermal Paints for Shock/Boundary Layer Interaction in Inlet Flows," AIAA Paper 92-3626, July 1992.

[8]Liu, T., Campbell, B. T., and Sullivan, J. P., "Fluorescent Paint for Measurement of Heat Transfer in Shock/Turbulent Boundary-Layer Interaction," *Experimental Thermal and Fluid Science*, Vol. 10, No. 1, 1994, pp. 101–112.

[9]Ragsdale, W., and Boyd, C., "Hypervelocity Wind Tunnel 9 Facility Handbook," 3rd ed., NAVSWC TR 91-616, NSWCDD, Silver Spring, MD, July 1993.

[10]Burnett, D., and Lewis, M., "A Re-Evaluation of the Waverider Design Process," AIAA Paper 93-0404, Jan. 1993.

[11]Kammeyer, M., and Gillum, M., "Design Validation Tests on a

Realistic Hypersonic Waverider at Mach 10, 14, 16.5 in the Naval Surface Warfare Center Hypervelocity Wind Tunnel No. 9," Naval Surface Warfare Center, NSWCDD TR 93-198, Silver Spring, MD, May 1994.

[12]Hedlund, E., Hill, J., Ragsdale, W., and Voisinet, R., "Heat Transfer Testing in the NSWC Hypervelocity Wind Tunnel Utilizing Co-Axial Surface Thermocouples," Naval Surface Warfare Center, NSWC MP 80-151, Silver Spring, MD, March 1980.

[13]Ragsdale, W., "COAX Heat Gage Data Reduction," Naval Surface Warfare Center, NSWC K24 Memo, Silver Spring, MD, July 1987.

[14]Rabek, J. F., *Mechanisms of Photophysical Processes and Photochemical Reactions in Polymer—Theory and Applications*, Wiley, New York, 1980, Chap. 1.

[15]Campbell, B. T., "Temperature Sensitive Fluorescent Paints for Aerodynamics Applications," M.S. Thesis, School of Aeronautics and Astronautics, Purdue Univ., West Lafayette, IN, 1993.

[16]Patankar, S. V., *Numerical Heat Transfer and Fluid Flow*, Hemisphere, New York, 1980, pp. 54–59.

[17]Lee, H., "Rapid Measurement of Thermal Conductivity of Polymer Films," *Review of Scientific Instruments*, Vol. 53, No. 6, 1982, pp. 884–887.